Environmental Science: Atmospheres

ROYAL SOCIETY OF CHEMISTRY

PAPER

View Article Online
View Journal | View Issue

Cite this: *Environ. Sci.: Atmos.*, 2023, **3**, 816

Aqueous-phase photochemical oxidation of water-soluble brown carbon aerosols arising from solid biomass fuel burning†

Vikram Choudhary, [ab] Max Loebel Roson,[a] Xinyang Guo,[a] Tania Gautam,[a] Tarun Gupta *[b] and Ran Zhao *[a]

Biomass burning is a major source of short-lived climate forcers, *e.g.*, brown carbon (BrC), that absorb solar radiation and cause warming of the Earth's atmosphere. A large fraction of the population in developing countries is still dependent on wood and animal dung cake burning for household cooking and heating. While wood burning emissions are well studied, a lack of understanding about animal dung burning emissions still persists. This is the first study to explore the aqueous-phase photochemical aging of laboratory-generated water-soluble brown carbon (WS-BrC) aerosols arising from cow dung cake burning, with a focus on cloud-water photochemistry. A comparison with wood burning (pine) was also carried out. We observed that WS-BrC arising from different types of solid biomass fuel burning encountered different evolution pathways, albeit similar UV-light was used during direct photolysis. The photo-enhancement in WS-BrC absorbance was induced more effectively upon exposure to UV-light with shorter wavelengths and coincided with oligomer formation during direct photolysis. During OH oxidation, WS-BrC emitted from burning of all three solid biomass fuels followed similar evolution pathways, with their second-order rate constant values being $(25.4 \pm 3.9) \times 10^8$, $(19.2 \pm 13.1) \times 10^8$ and $(23.3 \pm 6.5) \times 10^8$ M^{-1} s^{-1} for WS-BrC arising from burning of Indian cow dung, Canadian cow dung and pine wood, respectively. Combined with a few recent studies, these observations signify that the OH-oxidation lifetime of biomass burning WS-BrC aerosols in cloud-water may not depend on the biomass type.

Received 5th November 2022
Accepted 21st February 2023

DOI: 10.1039/d2ea00151a

rsc.li/esatmospheres

Environmental significance

South Asia is one of the most polluted and biomass burning dominated regions in the world. It is a major hotspot of anthropogenic atmospheric aerosol warming globally. Solid biomass fuel burning (*e.g.*, animal dung, wood, *etc.*) in this region affects climate substantially but has not been studied; for the first time, aqueous-phase atmospheric chemistry of light-absorbing pollutants from cow dung burning is investigated. We observed that the photo-enhancement was induced more effectively upon exposure to shorter wavelength UV-light during direct photolysis and it coincided with oligomer formation. Although different biomass burning types dominate the BrC budget in different regions globally, the fate of BrC in clouds/fog probably does not depend on biomass types implying robust and accurate estimations of climatic impacts.

1. Introduction

Brown carbon (BrC), a fraction of organic aerosols (OAs) known to show strong solar absorption in the ultraviolet (UV) spectrum and moderate absorption in the visible spectrum, is estimated to contribute significantly (~7 to 48%) to total global anthropogenic aerosol warming.[1–4] Besides climatic warming, strong absorption by BrC aerosols results in diminished UV solar radiation near Earth's surface, implying their important role in tropospheric photochemistry.[5,6] The characterization of BrC lifecycle parameters such as sources, sinks (aging mechanisms), optical properties and lifetime is paramount for global climate models to estimate their climatic impacts. However, the current understanding of these parameters is limited, causing large uncertainties in modelling results.[7–10]

Biomass burning, including wildfires,[11] agriculture residues[12] and solid biomass fuel burning,[13] has been identified as the dominant source of BrC aerosols globally; for example, ~50% of BrC absorption in southeastern USA,[3] ~80% in Delhi,[14] and ~35 to 70% in Beijing[15] have been attributed to biomass burning. Previous studies[7,16–19] have reported that biomass fuel

[a]*Department of Chemistry, University of Alberta, Edmonton T6G 2R2, Alberta, Canada. E-mail: rz@ualberta.ca*

[b]*Department of Civil Engineering and APTL at Center for Environmental Science and Engineering (CESE), Indian Institute of Technology Kanpur, Kanpur 208 016, India. E-mail: tarun@iitk.ac.in*

† Electronic supplementary information (ESI) available. See DOI: https://doi.org/10.1039/d2ea00151a.

types, their burning conditions and atmospheric aging processes can influence the chemical composition and optical properties of BrC. Therefore, to better understand and constrain the climatic impacts of biomass burning on the global scale, comprehensive characterization of the optical properties of BrC emitted during the combustion of different types of biomass from different geographical locations is crucial. For example, more than one billion of the global population, mainly from developing countries, is still using solid biomass fuel burning (*e.g.*, dung cakes, wood, *etc.*) as an affordable source of energy for cooking and heating.[20] As a matter of fact, ~60% of Indian and ~86% of African households were using solid biomass fuels for cooking and heating in 2016.[20] Moreover, at least 10–15% of Indian households (~150 million people) rely on dung cakes for cooking and heating implying their potentially substantial role in very poor air quality in India.[21] Burning such solid biomass fuels is often practiced with old and poorly designed burning devices, as such emissions arising from such fuels may be both more abundant and toxic than the fraction of households can indicate.[21,22] Previous studies (carried out between 2004 and 2015) have pegged the annual contribution of solid biomass fuel burning emissions to $PM_{2.5}$ (particulate matter with an aerodynamic diameter $\leq$ 2.5 μm) concentration from ~20 to 40% in India[23–25] and ~40% in Africa.[25] It is noted that OA is a predominant constituent (~40 to 60%) of the $PM_{2.5}$ load in India.[23,24,26,27] The majority of previous studies have focused on the aging of BrC aerosols produced by wood pyrolysis[16,28,29] and secondary BrC aerosols,[29,30] leaving other solid biomass fuel burning types, particularly dried animal dung cake burning, largely uncharacterized. It is imperative to recognize the similarities and differences in the environmental impacts induced by burning different solid biomass fuels.

Atmospheric aerosols, including BrC, subject to varying environmental conditions, *e.g.*, gas-phase, fog, clouds, *etc.*, during their atmospheric processing. The different atmospheric aging processes (*e.g.*, gas- and aqueous-phase photochemical oxidation, volatilization, *etc.*) can transform the chemical composition and optical properties of BrC aerosols following their emissions or formation.[7,9,31–33] Previous laboratory studies on aqueous-phase photochemical oxidation of secondary BrC showed rapid loss of chromophores also referred to as photobleaching.[29,30] However, photo-enhancement preceded photobleaching for biomass burning primary BrC aerosols.[16,28,29] These studies[16,28,29] observed that the photo-enhancement in BrC absorbance (and absorptivity) during aqueous photochemical oxidation stems from the formation of high molecular-weight chromophores (oligomers). It is noted that photochemical oxidation includes the effects of multiple aging processes, specifically, direct photolysis and OH oxidation. Different wavelengths of UV-light during these processes, especially direct photolysis, can have contrasting effects on BrC absorbance and composition. In this framework, it is observed that a majority of UV radiation reaching the Earth's surface is UVA (320 to 400 nm), and only 5% is UVB (290 to 320 nm).[34,35] A few recent studies have assessed the effects of UVB[16,28] and UVA[29] direct photolysis in an aqueous medium on BrC absorbance separately. However, a comparative analysis in conjunction with the effects of different wavelengths of UV-light on the evolution of BrC has never been done before.

The overall objective of this study was to comprehensively examine the evolution of BrC emitted from burning of solid biomass fuels during aqueous-phase photochemical oxidation processes. Specifically, we investigated: (a) changes in the absorbance, absorptivity and composition of laboratory-generated water-soluble brown carbon (WS-BrC) emitted from dung cakes and wood pyrolysis, (b) impact of the UV-light wavelength on the evolution of WS-BrC during direct photolysis; in particular, three different types of UV-lights were used, and (c) evolution in WS-BrC absorbance during aqueous OH oxidation for three solid biomass fuel burning types to examine their dependence on the biomass type. We note that the wavelength dependence of BrC photochemistry is poorly understood. In fact, the aqueous-phase photochemistry of BrC arising from dung burning has never been studied before.

2. Experimental methodology

2.1. BrC aerosol generation

Three types of solid biomass fuels, *i.e.*, firewood, dried cow dung cakes from a local Canadian farm (CAD) and cow dung cakes from India (IND), have been used in this study. The firewood, Lodgepole Pine (*Pinus Contorta*), was purchased from a local store. CAD samples were naturally dried cow dung cakes and were provided by Mattheis Ranch (an experimental farm managed by Rangeland Research Institute at the University of Alberta). IND samples (produced in India) were purchased through a major online shopping platform. The IND cakes were advertised as "pure cow dung" for spiritual and worship purposes. All solid biomass fuels samples were stored in a fume hood for drying.

Cellulose and lignin are the key components of biomass tissues. The pyrolysis of these components produces BrC chromophores such as phenols, nitrophenols, organic acids, *etc.*, that are highly prevalent in the ambient atmosphere.[28,36–39] Therefore, BrC aerosol particles were generated by the pyrolysis of the above-mentioned solid biomass fuels in a tube furnace, using the method described in Loebel Roson *et al.*,[37] in an aerobic atmosphere. Briefly, a small amount (<1 g) of each solid biomass fuel was placed in a quartz tube (internal diameter $= \frac{1}{2}$ inch) inside of a tube furnace (Carbolite Gero) and heated at a temperature of 500 °C. A constant air-flow of 0.2 slpm zero air (Parker Analytical Gas Systems, Model 64-01) was maintained through the quartz tube during the pyrolysis of solid biomass fuels. The setup is highly efficient in reproducing air flow and temperature heating profiles, which is difficult for open burning and smouldering setups. We note that our setup does not fully reproduce the combustion environment of actual solid biomass fuel burning. However, the BrC produced from pyrolysis should be a good representative of those emitted from real combustion. Similar tube furnace setups have been used in a number of recent investigations for biomass burning.[28,37,40–42] The aerosol particles emitted during the pyrolysis of different solid biomass fuels were collected onto 0.22 μm prebaked quartz filters (Whatman™; 47 mm diameter). The collected filters were stored in a freezer (−19 °C), usually for a week, until

chemical analysis. A total of four particulate-loaded filters for each solid biomass fuel burning ($n = 3$ for IND) and 2 blank filters were collected. The blank filters were generated by heating the furnace without any solid biomass fuel. The entire tube-furnace set-up was kept inside a fume hood to ensure safety. The schematic of the set-up is shown in Fig. S1.†

Furthermore, a quarter of each filter was extracted in deionized water (DI) by mechanical stirring for ~40 min. The IND and wood burning samples were extracted in 30 mL DI water, whereas the CAD burning filters were extracted in 25 mL DI water due to their lower particulate loading compared to the other two solid biomass fuel burning types. The blank filters were extracted in 25 mL DI water. Subsequently, the extracts were filtered through a 0.22 μm PTFE filter to remove the water-insoluble fraction of particulates.

2.2. Direct photolysis of WS-BrC

All the experiments examining direct photolysis of WS-BrC were carried out in a photoreactor. The photoreactor (Rayonet, PRP200) consists of a quartz vessel, placed at the center and surrounded by 5 UV-lamps. WS-BrC aqueous solution was contained in the quartz vessel and was continuously stirred with a magnetic stir bar throughout the experiments. Two different types of UV lamps, *i.e.*, UVB and UVA, were used. Additionally, UVB direct photolysis in a glass vessel was also examined. These experiments were referred to as UVB(Q), UVA(Q) and UVB(G) to distinguish between quartz and glass vessels. Photon flux spectra (cm^{-2} s^{-1} nm^{-1}) for these UV-lights were determined using a combination of direct emission spectrum measurements (Ocean Optics, USB2000 + ER) and chemical actinometry of 2-nitrobenzaldehyde (2NB).[43] More details about photon flux calculations are discussed in Section S1 of the ESI.† The photon flux spectra for all three UV-lights are shown in Fig. S2.† The flux spectra appeared polychromatic, with intensities peaking at 313 and 366 nm for UVB(Q) and UVA(Q) light, respectively (Fig. S2†). Overall, the predominant fraction of photon flux for these UV-lights fell within 280 to 400 nm wavelengths (Fig. S2†). The flux intensity of UVB(G) light also peaked at 313 nm; however, the glass vessel (compared to quartz) blocked shorter wavelength UVB flux (≤320 nm) quite efficiently (~50 to 90%) and the loss of flux at longer wavelengths (>320 nm) was very small. We employed UVB(G) as a strategy to filter out shorter wavelengths irrelevant to actinic solar photon flux (Fig. S2 and S3†). Furthermore, the integrated photon fluxes for all three UV-lights were also determined. The integrated flux was highest for UVA(Q) (*i.e.*, 4.7×10^{16} cm^{-2} s^{-1}) followed by UVB(Q) (*i.e.*, 2.8×10^{16} cm^{-2} s^{-1}) and UVB(G) (*i.e.*, 1.7×10^{16} cm^{-2} s^{-1}). An illumination time of 120 min was maintained during direct photolysis with aliquots being taken at 0, 10, 20, 30, 45, 60, 90 and 120 min for absorbance measurements and 0, 30, 60 and 120 min for mass spectrometric and total organic carbon (TOC) analyses (see below). A fan was used to cool the experimental solution. Still, the temperature of the aqueous solution rose up to ~40 °C after 120 min of irradiation. Previous studies[44,45] have shown that a change in temperature during photochemical oxidation processes has potential to impact the chemical mechanisms and kinetics of organic molecules. However, raising the temperature change from room temperature by 10 to 20 °C would not affect the composition and kinetics of organic compounds, including BrC chromophores, substantially.[46–48] As a matter of fact, variability in kinetic parameters would likely to be within 10% due to a temperature change of 20 °C, a very small change compared to the variability observed in this study.

2.3. OH oxidation of WS-BrC

The aqueous-phase OH oxidation experiments were performed with the same experimental apparatus utilized in the UVB(Q) direct photolysis experiment. The experiments were conducted at room temperature for 1 h with aliquots being taken at 0, 5, 10, 15, 20, 30, 45 and 60 min for absorbance measurements. Hydrogen peroxide (H_2O_2) 30% w/w (Sigma Aldrich) was added to WS-BrC aqueous solution to act as an *in situ* source of OH radicals upon exposure to UVB radiation in the quartz vessel during OH oxidation experiments. The added concentration of H_2O_2 in the aqueous solution varied from 7.5 mM to 125 mM, depending on the measured TOC concentration of each WS-BrC solution, to maintain a relatively consistent steady-state OH concentration ([OH]ss) similar to that in ambient cloud water ($\sim 10^{-13}$ M). The added H_2O_2 concentrations may look very high compared to the ambient quantity, yet it is the [OH]ss that governs the photochemistry and crucial to determine the WS-BrC lifecycle parameters such as photochemical decay, lifetime, *etc.* in an aqueous medium. Therefore, pimelic acid was used as a probe compound to quantify [OH]ss in this study.[49] Each extract was spiked with 10 μM pimelic acid and its degradation during aqueous-phase OH oxidation was monitored using liquid chromatography-mass spectrometry (LC-MS). Further details about the method are discussed in Section S2, Fig. S4 of the ESI† and Section 3.5.

However, there might be a potential bias in aqueous-phase OH oxidation of WS-BrC due to the reaction between carbonyl compounds and H_2O_2. The carbonyl compounds can react with H_2O_2 *via* a nucleophilic addition of H_2O_2 to a carbonyl compound, but carbonyl carbon must be an efficient electrophile for this reaction to proceed.[50–52] Aromatic compounds with functional groups such as phenols, carbonyls, aldehydes, *etc.*, have been identified as the predominant constituents of biomass burning emissions.[37–39] However, due to the electron donating nature of aromatic rings, aromatic carbonyls are less reactive towards nucleophilic addition reactions. In fact, a recent study[53] has found the nucleophilic additions of water to aromatic carbonyls to be negligible. A few dark control experiments were carried out in this study to confirm that the reactions between H_2O_2 and WS-BrC constituents (especially with the carbonyl functional group) under dark conditions (*i.e.*, no UVB illumination), if any, do not alter WS-BrC optical properties.

2.4. UV-visible spectrophotometer measurements

The measurements of WS-BrC absorbance in the aqueous extracts were based on the Beer–Lambert law. A multi-channel UV-vis spectrophotometer (Genesys; Model: 10S Vis spectrophotometer) with a path length of 1 cm was used for the

measurements. Although the spectrophotometer can measure absorbances from 325 to 1100 nm, only 330 to 700 nm absorbance data were utilized in this study to minimize matrix interference from compounds such as nitrates, which absorb at wavelengths < 340 nm.[3,54] These absorbance measurements were further utilized to calculate absorption properties, specifically, mass absorption efficiency ($MAE_{WS\text{-}BrC\text{-}\lambda}$) and solar-weighted total absorbance for WS-BrC from 330 to 500 nm. The MAE of WS-BrC, expressed in $m^2\ g^{-1}$-C, at a given wavelength ($MAE_{WS\text{-}BrC\text{-}\lambda}$) was calculated using eqn (1)[19]

$$MAE_{WS\text{-}BrC\text{-}\lambda} = \frac{A_{WS\text{-}BrC\text{-}\lambda} \times \ln(10)}{l \times WSOC} \quad (1)$$

where $A_{WS\text{-}BrC\text{-}\lambda}$ is the absorbance of WS-BrC at a given wavelength (λ), l is the path length of the spectrophotometer (*i.e.*, 0.01 m) and WSOC is the concentration of water-soluble organic carbon in mg-C L^{-1}. WSOC (along with total nitrogen (TN)) concentrations were measured using a TOC-TN analyzer (Shimadzu TOC-L CPH Analyzer). The details of the method are discussed in Section S3 of the ESI.†

The assessment of the absorption properties of WS-BrC aerosols at a single wavelength (*e.g.*, 365 nm) might not be sufficient to understand their evolution during photochemical oxidation.[32,55] Therefore, the solar-weighted total absorbance, integrated from 330 to 500 nm, was also assessed in this study. It is noted that the absorbance values of freshly emitted WS-BrC from all three solid biomass fuel burning types were negligible beyond 500 nm and thus, not considered in the calculation of solar-weighted total absorbance. The calculations are discussed in more detail in Section S4 of the ESI.†

2.5. MS analyses

To obtain the molecular composition, the water extracts of each solid biomass fuel burning sample and blanks were subjected to non-targeted analysis on a high-resolution LC-MS (Agilent 6220 oaTOF system). Positive and negative electrospray ionization (ESI^+ and ESI^-, respectively) techniques were employed. These techniques are good at detecting compounds such as phenols, nitrophenols *etc.* without their extensive fragmentation.[28,38,56] Water (solvent A) and Acetonitrile (solvent B), both buffered with 0.05% formic acid, were used as solvents for the binary mobile phase during LC-MS measurements. The mobile phase was delivered at a flow rate of 0.3 mL min^{-1} for a total runtime of 30 min. The mobile phase composition for the first minute of the run was 90% A and 10% B. B was ramped up to 20% from 1 to 3 min, ramped up to 95% from 3 to 26 min, held at 95% from 26 to 29 min and ramped down to 10% from 29 to 30 min. The separation of the compounds was performed using a Luna Omega 3 μm Polar C18 column (150 × 2.1 mm; Phenomenex Inc.). However, the column could only reliably separate monoaromatic compounds, and only a handful of them were subsequently detected in ESI^+ mode. Thus, only ESI^- mode was considered in this study. We also performed high-resolution LC-MS measurements for a couple of blank filters. The ESI^- mode MS spectra for blank filters were found to be clean with a very small background signal. The analysis and molecular formula assignment of high-resolution LC-MS data were performed using MassHunter software (v. B.07.00).[37] An aqueous mixture containing 10 mM of each standard compound (*viz.*, vanillin, sinapaldehyde, coniferyl aldehyde, 4-nitroguaiacol and 4-nitrocatechol) was analyzed on a high-resolution LC-MS using the same parameters as the solid biomass fuel burning samples (Table S1†) to ensure efficacy and correct molecular formula assignments from MassHunter.

Size-exclusion chromatography (SEC) is a more common technique to investigate the formation of high molecular-weight compounds (oligomer).[16,57,58] However, in this study, a direct flow-injection MS (Thermo Fisher Scientific model LTQ-XL) was used to identify oligomer formation during aqueous-phase direct photolysis. The MS sensitivity in this technique is susceptible to changes due to the suppression of the ionization signal from matrix interference, such as structural complexity, loading/concentration of analyte solution, *etc.* The use of an internal standard during the flow-injection can account for this ionization suppression. However, oligomers (dimers) are likely to be multifunctional compounds, and therefore using only a single-functional compound (pimelic acid) to account for their ionization suppression may not be enough. In this context, a previous study[59] compared the ionization suppression effect of both single-functional (*e.g.*, aniline, lauric acid, 2-methylquinoline, *etc.*) and multifunctional internal standards (*e.g.*, gemfibrozil) in complex sample matrices (*e.g.*, waste water) and found bias to be within ± 15%. Additionally, several studies[60–62] have used single-functional compounds as an internal standard to identify a range of compounds in complex sample matrices during direct flow-injection MS analysis.

In this work, pimelic acid (m/z = 159.15) was used as an internal standard during flow-injection MS analysis. Two samples each for pine wood and IND dung burning were analyzed. The total runtime for the experiment was 10 min and the flow-injection flow rate was 0.005 mL min^{-1}, achieved with a syringe pump. The signal intensity for all the compounds in the monomer region (m/z < 210)[28] and dimer region (m/z = 250 to 350)[28,63] were normalized to that of pimelic acid (10 μM), an internal standard used to account for ionization suppression. The % change in the ratio was found to be within ± 10% (discussed in Section 3.4) signifying the efficacy of pimelic acid as an internal standard in this study. Furthermore, a LTQ XL LC-MS was also used to identify and monitor pimelic acid degradation for the quantification of [OH_{ss}]. The compounds with carboxylic and phenolic groups are easily detectable in ESI^- mode. Thus, ESI^- mode was used for monitoring of pimelic acid. The separation column, mobile phase and method used during the measurements were identical to those of the high-resolution LC-MS measurements discussed above. The data from the Thermo Scientific LC-MS were analyzed using FreeStyle™ 1.8 software.

3. Results and discussion

3.1. Absorptivity of WS-BrC from different solid biomass fuel burning

$MAE_{WS\text{-}BrC}$, also referred to as absorptivity, indicates the mass normalized absorption cross-section of WS-BrC chromophores.

The absorptivity values of WS-BrC emitted from dung cakes (both IND and CAD) and pine wood burning, calculated by utilizing WS-BrC absorbance and WSOC concentrations (Table S2†) in eqn (1), were determined at 365 nm and 400 nm. We observed that the absorptivity values of WS-BrC aerosols from dung cake burning (averaged at ~0.75 and 0.30 m^2 g^{-1}-C at 365 nm and 400 nm, respectively) were ~2 to 3 times higher than that of pine wood burning (Fig. S5†). In this context, previous studies[18,19,28,37,56] have reported that nitrogen containing organic compounds govern the optical properties (*e.g.*, absorptivity) of biomass burning BrC. In this study, a higher water-soluble organic nitrogen (WSON) over WSOC (WSON/WSOC) ratio was observed for dung cake burning than pine wood (Table S2†). A recent mass-spectrometry based study[37] also observed higher prevalence of nitrogen containing OA in dung cake burning than wood burning. This probably explains the higher absorptivity values for dung cake burning WS-BrC than pine wood. Furthermore, previous studies[12,13,16,19,28,29,37,64,65] observed a large variability in the absorptivity values of biomass burning WS-BrC. For example, the absorptivity values at 365 nm varied from 0.7 to 1.5 m^2 g^{-1}-C for dung cake burning,[13,28,37,64,65] 0.1 to 2.0 m^2 g^{-1}-C for wood burning,[16,19,28,29,37] and 1.2 to 3.0 m^2 g^{-1}-C for agriculture-residue burning.[12,65] The absorptivity values observed in our study fell on the lower side of the ranges reported by these studies and it could be the result of different types of burning set-ups (discussed in Section 2.1) utilized for burning in this study.

3.2. Absorption changes induced by direct photolysis

Fig. 1 highlights spectral changes in the WS-BrC absorbance and absorptivity of IND dung, CAD dung and pine wood burning during aqueous-phase direct photolysis using UVB(Q) and UVA(Q) light. It is noted that the changes in WSOC concentration during photolysis were very small (within 15%) and therefore not considered in absorptivity calculations. We observed that the nature and scale of changes occurring in WS-BrC absorbance and absorptivity were distinct for each solid biomass fuel burning even though identical UV-light exposure was used during photolysis (Fig. 1). For example, during UVB(Q) photolysis, WS-BrC from all three solid biomass fuel burning types exhibited varying scale of photo-enhancement in the visible region. However, in the near UV-region, IND dung burning WS-BrC underwent photobleaching, CAD dung

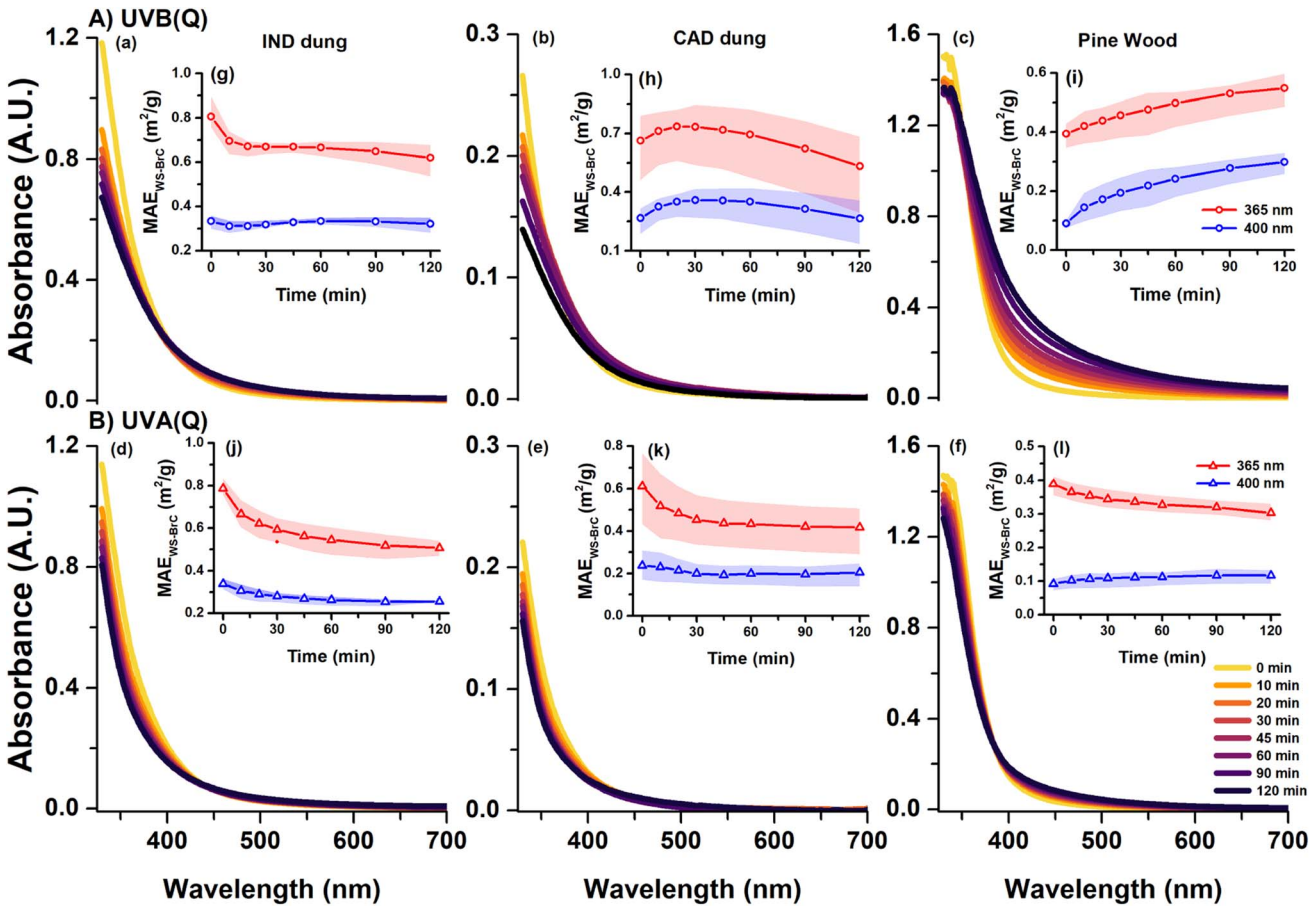

Fig. 1 Spectral change in absorbance from 330 to 700 nm of WS-BrC emitted from pyrolysis of IND dung (a and d), CAD dung (b and e) and pine wood (c and f) during aqueous-phase direct photolysis using UVB(Q) (panel A) and UVA(Q) (panel B) light, where (Q) denotes an experiment performed with a quartz vessel. The color code of absorption spectra indicates the length of irradiation. The inset plots indicate changes in mass absorption efficiency (MAE_{WS-BrC}) at 365 and 400 nm for the corresponding fuels. The MAE_{WS-BrC} changes at 365 and 400 nm act as case studies of the changes in the near UV-region and visible region, respectively.

burning underwent temporary photo-enhancement followed by photobleaching, and pine wood burning only encountered intense photo-enhancement (Fig. 1A). In contrast, during UVA(Q) photolysis, all three solid biomass fuel burning types underwent varying scale of photobleaching in the near UV region, whereas, in the visible region, WS-BrC from both dung cake burning underwent a combination of photobleaching (at shorter wavelengths, 400 to 425 nm) and photo-enhancement (at longer wavelengths, 425 to 550 nm), but only photo-enhancement (scale was smaller compared to UVB(Q)) was observed for pine wood burning (Fig. 1B). A few recent studies based on aqueous-phase UVB(Q) photolysis of laboratory-generated WS-BrC aerosols from pine wood burning[28] and cherry hardwood burning[16] also observed photo-enhancement in their absorbance and absorptivity. It should be noted that this is the first study to assess aqueous-phase photochemical oxidation of WS-BrC from dung cake burning. Furthermore, to quantify and compare the overall impact of these photolysis processes on WS-BrC from these solid biomass fuel burning types, we assessed % change in their solar-weighted total absorbance (Fig. S6†). The observations from all these analyses appeared to suggest that the WS-BrC from different solid biomass fuel burning types might follow different evolution pathways albeit during a similar direct photolysis process. Moreover, these observations signified that the degree of photo-enhancement in WS-BrC absorbance would likely be more intense during photolysis by shorter wavelength UV-light, whereas photobleaching dominates under longer wavelength UV-light. Furthermore, it is well known that the absorptivity of BrC is also highly wavelength-dependent; therefore, direct photolysis of BrC is governed by a function that is more complex than the photon flux. Thus, a case study was designed by simulating the action spectra of pine wood burning WS-BrC as a function of wavelength (more details are given in Section S1 and Fig. S3 of the ESI†). We obtained that the direct photolysis of WS-BrC was more pronounced under exposure to UVB(Q) than UVA(Q). However, the integrated photon flux was higher (~2 times) for UVA(Q). These observations further signify a more prominent role of shorter wavelength UV-light in direct photolysis.

3.3. Impact of the UV-light wavelength during direct photolysis

To corroborate the hypothesis that UV lights with shorter wavelengths give rise to the observed photo-enhancement, we also explored the UVB photolysis of IND dung and pine wood burning samples in a glass vial (referred to as UVB(G)) and compared them with the UVB(Q) and UVA(Q) experiments (Fig. 2). We observed that photobleaching, if occurring (*e.g.*, IND dung burning; Fig. 2a and b), was most intense during UVA(Q) followed by UVB(G) and UVB(Q) in that order. In contrast, the photo-enhancement – if occurring (*e.g.*, pine wood burning; Fig. 2c and d) – was most intense during UVB (Q) followed by UVB (G) and UVA (Q) in that order. It is noted that the simulated

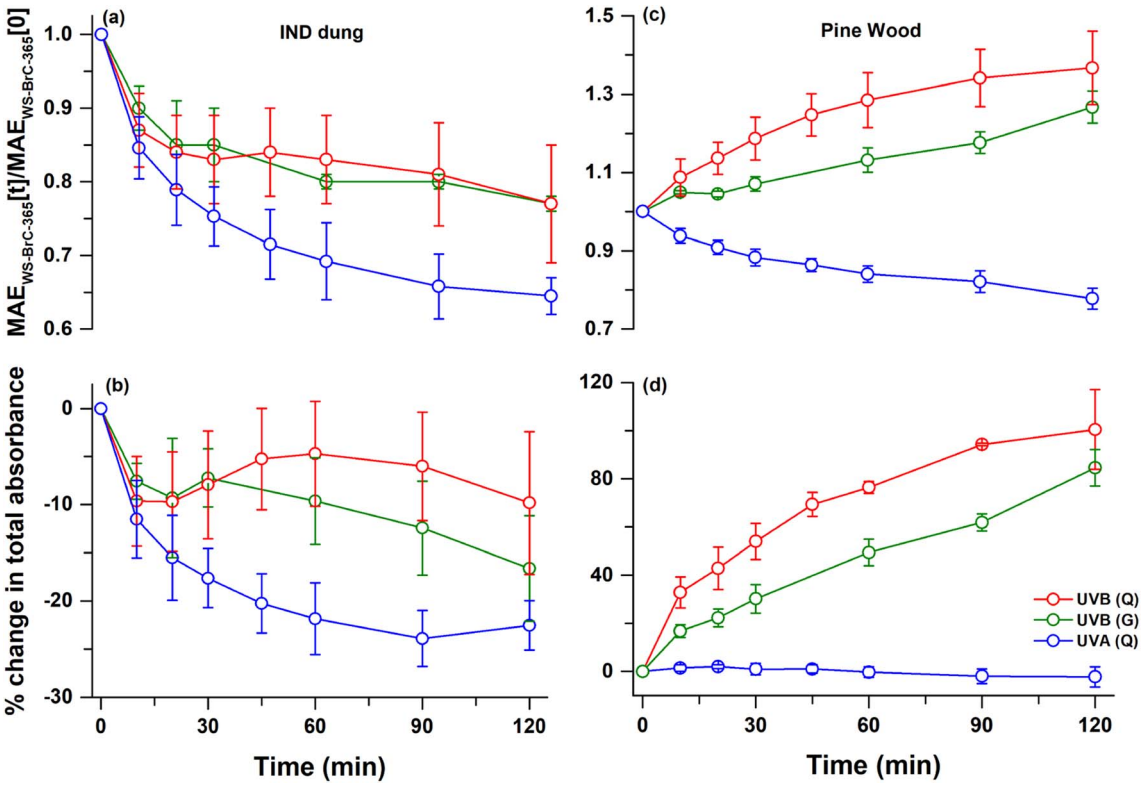

Fig. 2 Comparison of temporal variations in $MAE_{WS\text{-}BrC\text{-}365}$ normalized to their initial value ($MAE_{WS\text{-}BrC\text{-}365}[t]/MAE_{WS\text{-}BrC\text{-}365}$ [0]) and % change in total absorbance of IND dung burning (a and b) and pine wood burning (c and d) WS-BrC during aqueous-phase direct photolysis using three different types of UV-lights, where (Q) and (G) denote experiments performed with a quartz vessel and a glass vial, respectively.

wavelength-specific direct photolysis rates, also referred to as action spectra, of WS-BrC during UVB(G) exposure were found to be ~1/3rd of that during UVB(Q) (Fig. S3†). However, the integrated photon fluxes for both UVB(Q) and UVB(G) were comparable as discussed in Section 2.2 (Fig. S2†). These observations further corroborate our hypothesis discussed above. Additionally, we acknowledge that the direct photolysis rates of WS-BrC corresponding to different UV-lights used in this study were significantly higher than actinic solar photon flux (Fig. S3†). However, the objective of this study was to systematically investigate the impact of the wavelength on the photochemistry of BrC. We found that photon flux spectra ranging from 320 to 380 nm, best reflected by UVB(G) and UVA(Q) lights, would most likely govern the direct photolysis of WS-BrC in aqueous media such as clouds and fog droplets.

3.4. Potential formation of oligomers

Biomass burning emissions are highly enriched in aromatic compounds, such as phenols, nitrophenols, carbonyls, organic acids, *etc.*[37–39] These conjugated compounds, especially monoaromatics, form oligomers through radical coupling reactions involving either an oxygen atom (of the hydroxyl functional group) or a carbon atom (of the aromatic ring) during aqueous-phase photochemical oxidation processes.[63,66] The oligomerization of conjugated compound/s causes it to become larger in size (increase in the molecular weight) resulting the energy required for the π–π^* transition to become narrower and the wavelength of light absorbed by the oligomer correspondingly becomes longer.[7]

In this study, WS-BrC aerosols from different solid biomass fuel burning types (mainly pine wood burning) underwent varying degrees of photo-enhancement (particularly in the visible region) during aqueous-phase direct photolysis as discussed in previous sections. The corroboration and extent of oligomer formation during photolysis of dung cakes and pine wood burning WS-BrC may potentially substantiate the relationship between oligomer formation and photo-enhancement.

To ascertain the potential formation of oligomers in this study, several offline chemical analyses (*e.g.*, high-resolution ESI^- LC-MS, WSOC and direct MS flow-injection) were performed on samples collected during aqueous-phase UVB(Q) and UVA(Q) direct photolysis. The most dominant peaks in the ESI^- base peak chromatograms (BPCs) of these solid biomass fuel burning water-extracts eluted between 2 and 14 min, and almost all of them were associated with C6 to C10 monoaromatic compounds, as listed in Table S3.† During direct photolysis, these BPC peaks dissipated much faster upon exposure to UVB(Q)-light (Fig. S7a†) rather than UVA(Q)-light (Fig. S7b†). As a matter of fact, the total intensity of monoaromatic compounds reduced by ~80 to 100% after 120 min of UVB(Q) photolysis. However, the observed loss in monoaromatics was within ~20% during UVA(Q) photolysis (Fig. S7c†). Meanwhile, the observed loses in WSOC concentration during both UVB(Q) and UVA(Q) direct photolysis were similar and within ~15% (Fig. S7c and S8†). The comparatively faster disappearance (~4 to 5 times) of monoaromatic compounds during UVB(Q) direct photolysis compared to UVA(Q), but similar changes in WSOC concentrations, indicates the possibility of monoaromatic compounds reacting with each other through radical coupling reactions[63,66] and forming dimeric compounds (oligomer structures) upon exposure to UVB-light, which we investigate further in the following section.

To further corroborate the formation of oligomers, we utilized direct flow-injection MS on photolyzed aliquots of pine wood burning (Fig. 3 and S9†) and IND dung burning (Fig. S10†) water-extract samples from UVB(Q) and UVA(Q) experiments. The signals of all detected peaks were normalized against the signal of the internal standard (*i.e.*, pimelic acid, $m/z = 159.15$). For pine wood burning, we observed a decreasing trend in direct flow-injection MS signal intensity during both UVB(Q) (Fig. 3a–c) and UVA(Q) (Fig. 3d–f) photolysis. During UVB(Q) photolysis, the decrease in the total MS signal intensity in the monomeric region ($m/z = 100$ to 215) was much faster than in the dimeric region ($m/z = 215$ to 350). However, the decrease in the monomeric and dimeric regions appeared to be nearly similar during UVA(Q) photolysis. In this regard, previous studies have also shown that biomass burning organic aerosols undergo both formation[16,28,29] of high molecular-weight compounds (oligomers) and loss[16,29,67] of a few existing ones simultaneously during aqueous-phase photochemical oxidation processes. We have attempted to identify individual dimer peaks formed during the direct photolysis under UVB(Q); however, it was proven challenging due to the small signal intensities. Instead, we took an alternative approach and obtained the total signal over the dimeric and monoaromatic regions. Furthermore, we assessed and compared the temporal variations in % change in the ratio of the total MS signal intensity over the dimeric and monoaromatic regions (Fig. 3g and Table S4†). We observed that the ratio consistently increased (~35% after 120 min) upon exposure to UVB(Q) photolysis. However, it decreased (~10 to 15% after 120 min) during UVA(Q) photolysis (Fig. 3g) signifying that potential formation of oligomers may be higher during UVB(Q) photolysis than UVA(Q). The standard deviation of % change in the ratio was within $\pm$ 10% indicating the efficacy of the method in identifying oligomer formation qualitatively. For IND dung burning, we hardly observed any significant MS signal in the dimeric region (Fig. S10†), indicating that oligomeric compounds were formed to a lesser extent compared to pine wood burning. The consistency observed between the potential oligomer formation and the absorbance behavior of pine wood and IND dung burning WS-BrC during direct photolysis in this study substantiates their relationship.

In summary, these observations signify two major findings: firstly, oligomer formation would be more likely during exposure to shorter wavelength UV-light. While previous studies used either UVB or UVA as light sources, our study represents the first direct comparison of the two. Secondly, the chemical structure of monomers and their abundance would be the driving factors for oligomerization during aqueous-phase direct photolysis. For example, previous studies have reported that monoaromatic compounds, such as guaiacol,[28] vanillin,[66] syringol,[63] and coniferyl aldehyde[66] can react with each other and form light-absorbing oligomers during aqueous-phase UVB(Q) direct photolysis. These monoaromatic compounds (except syringol) were observed in emissions of all three solid

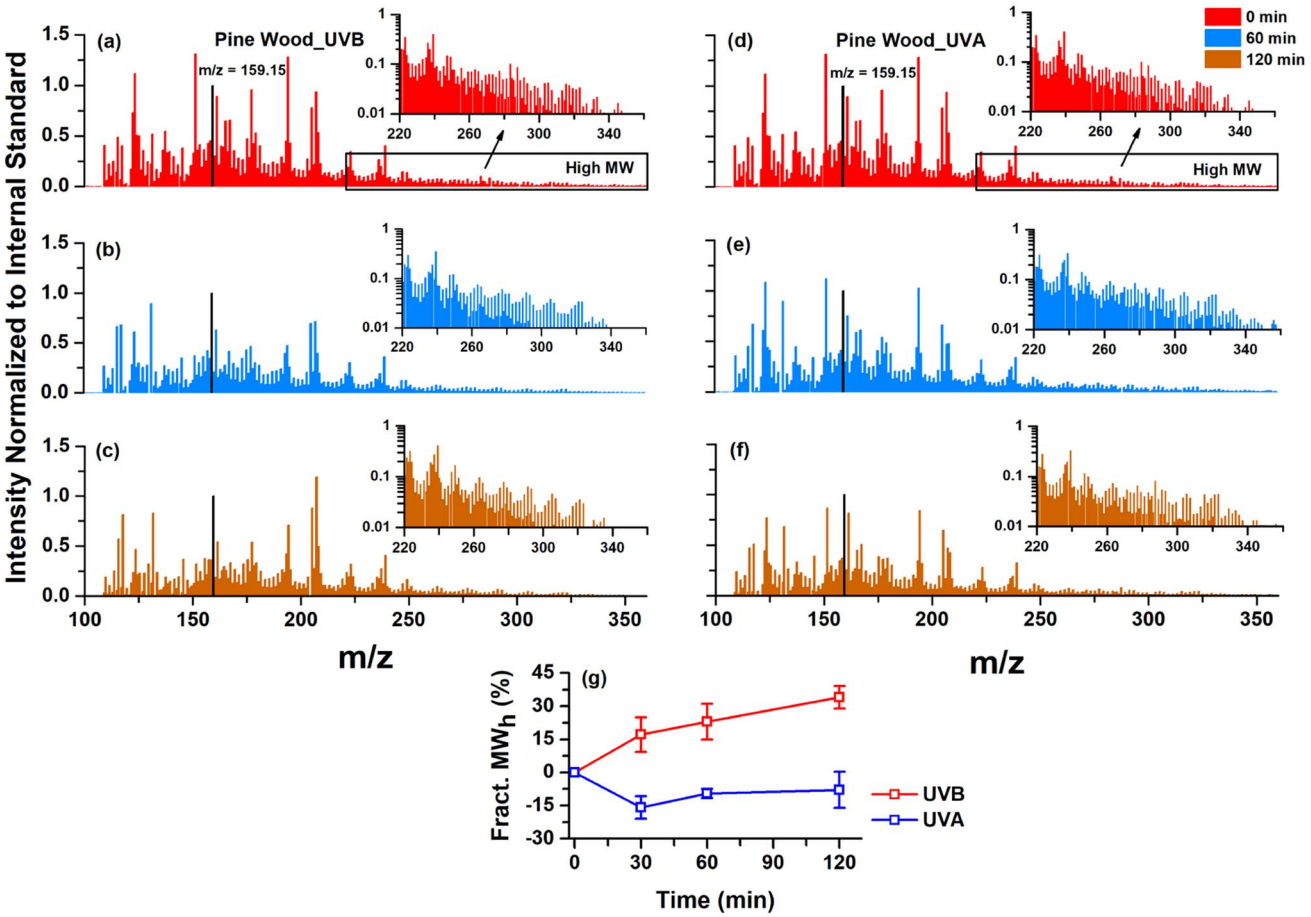

Fig. 3 Temporal variation in direct flow-injection MS spectra at 0, 60 and 120 min for pine wood burning during UVB(Q) (a, b and c) and UVA(Q) (d, e and f) direct photolysis experiments normalized using an internal standard. Also shown is % change in the ratio of total direct MS intensity of higher (m/z = 215–350) and lower (m/z = 100–215) molecular-weight compounds (g). The black bar is the normalized signal of the internal standard (*i.e.*, pimelic acid, m/z = 159.15).

biomass fuel burning types in this study (Table S5†). It is noted that we did not observe syringol in our study; however, it has been reported to be a good tracer for wood burning.[68] Additionally, the emissions of these monomers from wood burning were ~2 to 4 times higher than IND dung burning in our study (Table S5†). A recent study[37] has also reported that wood burning emissions are highly rich in lignin-degradation products (monomers) compared to animal dung cakes. The enrichment of such monoaromatic compounds is likely responsible for the more profound photo-enhancement in pine wood burning WS-BrC than dung burning observed in this study. Unfortunately, the method we employed did not allow molecular-level identification of oligomers that are responsible for the observed photo-enhancement. In future studies, instruments and methods better suited for oligomer detection – *e.g.*, SEC, MS coupled with different ionization sources – should be employed to confirm our observation.

3.5. OH oxidation

Photobleaching was a common characteristic during aqueous-phase OH oxidation of WS-BrC aerosols emitted from dung cake and pine wood burning. The changes in WS-BrC absorbance at 365 nm – normalized to its value at the beginning of the experiment – for all the solid biomass fuel burning types corroborate this characteristic, as presented in Fig. 4. The absorbance changes occurring during the dark control (*i.e.*, H_2O_2 + no UVB light) were negligible, as expressed by the black dashed lines in Fig. 4. The effect of direct photolysis (*i.e.*, no H_2O_2 + UVB light) on WS-BrC absorbance, expressed by the blue dashed lines, was more complex as discussed in the previous sections. Accelerated photobleaching in WS-BrC absorbance was observed during OH oxidation for all the solid biomass fuel burning types, as presented by the red solid lines. The mean ± standard deviation values of [OH]ss concentrations during OH oxidation experiments were $(1.8 \pm 0.7) \times 10^{-13}$, $(5.7 \pm 1.2) \times 10^{-13}$ and $(1.3 \pm 0.7) \times 10^{-13}$ M for IND dung, CAD dung and pine wood burning, respectively.

The bleaching/enhancement rate in WS-BrC absorbance was calculated assuming that the evolution of absorbance in the aqueous system was pseudo first-order (Fig. 4). The pseudo first-order effective OH oxidation rate constant ($k^{I}_{OH,eff}$) was calculated by subtracting the observed pseudo first-order rate constant during dark control (k^{I}_{ctl}) and direct-photolysis

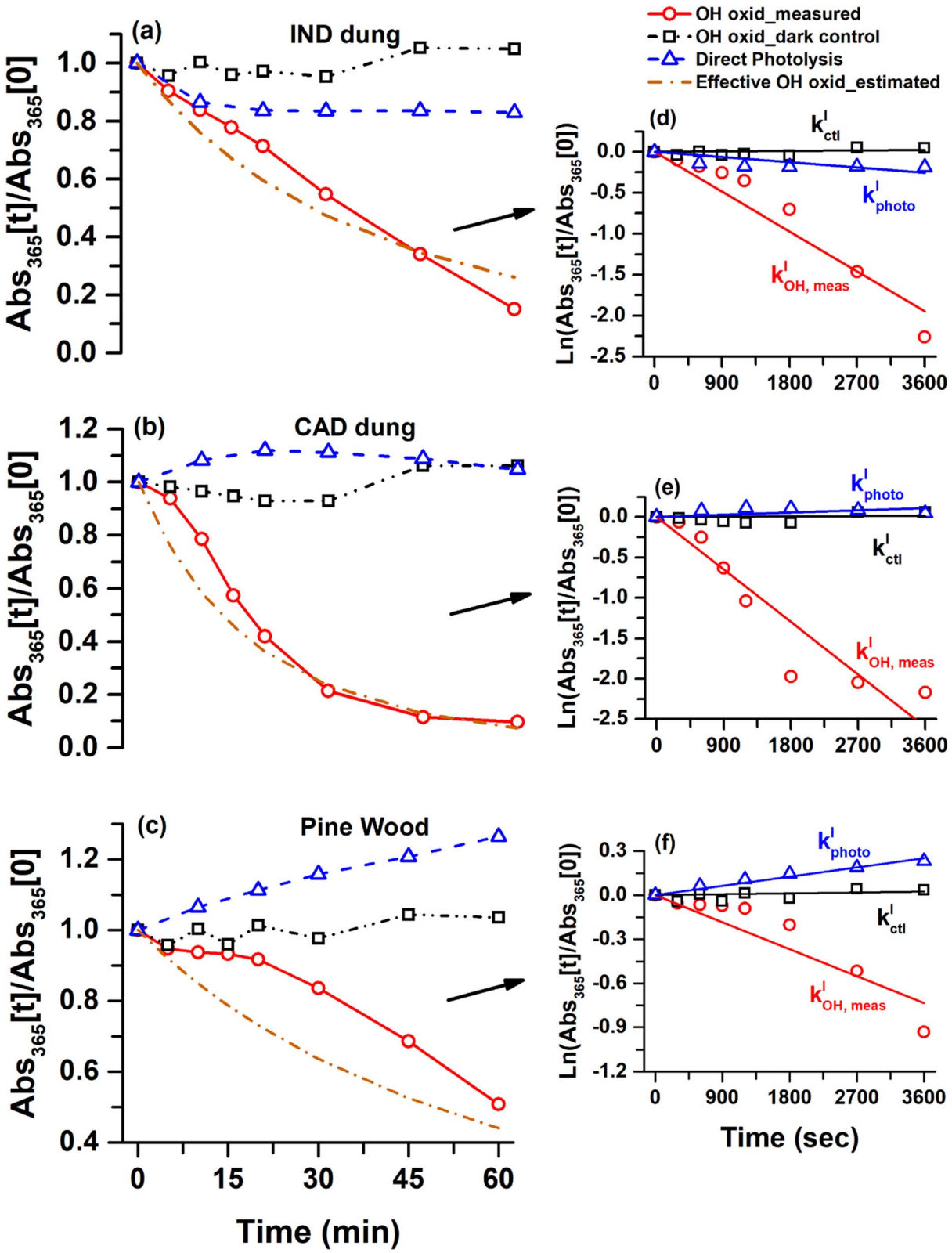

Fig. 4 Temporal profiles of absorbance at 365 nm normalized to their initial value ($Abs_{365}[t]/Abs_{365}[0]$) during aqueous-phase OH oxidation (red), dark control (black) and direct photolysis (blue) experiments for WS-BrC emitted from IND dung (a and d), CAD dung (b and e) and pine wood burning (c and f). The plots (a), (b) and (c) indicate the photochemical decay/enhancement profiles of $Abs_{365}[t]/Abs_{365}[0]$, whereas (d), (e), and (f) indicate the corresponding first-order decay/enhancement plots for WS-BrC. The brown colored dashed lines indicate simulated decay due to OH oxidation only ($k^{II}_{OH,eff}$).

Table 1 Aqueous-phase second-order rate constants and estimated cloud-water half-life of WS-BrC emitted from the pyrolysis of different solid biomass fuels, calculated from absorbance at 365 nm

Origin/Type	$k^{II}_{OH,meas}$ [a] (M^{-1} s^{-1}; $\times 10^8$)	$k^{II}_{OH,eff}$ [b] (M^{-1} s^{-1}; $\times 10^8$)	$\tau_{1/2,\ cloud\text{-}water}$ [c] (min)
IND dung	29.9 ± 3.4	25.4 ± 3.9	67 ± 10
CAD dung	18.7 ± 13.2	19.2 ± 13.1	129 ± 66
Pine wood	15.9 ± 5.5	23.3 ± 6.5	78 ± 24
Cherry hardwood[16]	—	29.0 ± 5.0	~58
Imine BrC[30]	—	12–210	5–98

[a] Corrected for the dark (H_2O_2) control. [b] Corrected for contribution due to dark control and UVB direct photolysis. [c] Estimated corresponding to $k^{II}_{OH,eff}$ and by assuming ambient cloud-water with an [OH]ss of 1×10^{-13} M, representing the upper band of OH in remote cloud-water.[45]

(k^{I}_{photo}) from the OH oxidation rate constant ($k^{I}_{OH,meas}$) as expressed by eqn (2). The second-order effective OH oxidation rate constant ($k^{II}_{OH,eff}$) was calculated using eqn (3) as given below:

$$k^{I}_{OH,eff} = k^{I}_{OH,meas} - k^{I}_{photo} - k^{I}_{ctl} \quad (2)$$

$$k^{II}_{OH,eff} = \frac{k^{I}_{OH\ ,\ eff}}{[OH]ss} \quad (3)$$

The $k^{II}_{OH,eff}$ for WS-BrC - calculated corresponding to changes in absorbance at 365 nm - was $(25.4 \pm 3.9) \times 10^8$, $(19.2 \pm 13.1) \times 10^8$ and $(23.3 \pm 6.5) \times 10^8$ M^{-1} s^{-1} for IND dung, CAD dung and pine wood burning, respectively (Table 1). These $k^{II}_{OH,eff}$ values were further utilized to estimate and simulate changes in WS-BrC absorbance due to OH oxidation only, shown by the brown colored dashed lines in Fig. 4. Interestingly, the near similar values of $k^{II}_{OH,eff}$ for different types of solid biomass fuel burning (Table 1) indicate that the second-order OH oxidation rate constant might not depend on the biomass type. A recent study[16] has also reported a near similar $k^{II}_{OH,eff}$ of $(29.0 \pm 5.0) \times 10^8$ M^{-1} s^{-1} for cherry hardwood burning WS-BrC (Table 1) bolstering our observations. Another study[69] found comparable $k^{II}_{OH,eff}$ values, ranged from (37–52) $\times 10^8$ M^{-1} s^{-1}, for nitrophenols. It is noteworthy that nitrophenols are an important class of WS-BrC chromophores that originate from biomass burning.[38,39,70] However, the $k^{II}_{OH,eff}$ values for secondary BrC arising from reactions between di-carbonyls and ammoniums sulfate (imine BrC) were reported to be significantly different from biomass burning, ranging from (12 to 210) $\times 10^8$ M^{-1} s^{-1} (Table 1).[30]

Additionally, to explore the fate of WS-BrC aerosols in aqueous media such as clouds and fog droplets, we estimated their cloud-water half-life ($\tau_{1/2,\ cloud\text{-}water}$) based on changes in absorbance at 365 nm due to OH oxidation only. The half-life indicates time taken for WS-BrC absorbance to reach half of its initial value and was calculated using eqn (4)[44,71]

$$\tau_{1/2,\ cloud\text{-}water} = \frac{1}{\left(k^{II}_{OH,eff} \times [OH]ss\right)} \quad (4)$$

We assume ambient cloud-water with an [OH]ss of 1×10^{-13} M, representing the upper band of remote cloud-water.[45] We note that the in-cloud time of an air mass can vary significantly. Nonetheless, the values shown in Table 1 serve as a direct comparison between fuel types. The half-life values of WS-BrC from different solid biomass fuel burning types, ranging from ~60 to 120 min, appeared to be comparable (Table 1). However, the $\tau_{1/2,\ cloud\text{-}water}$ values for imine BrC were quite different from biomass burning and showed a large variability from ~5 to 100 min (Table 1). Furthermore, the evolution of WS-BrC during direct photolysis was found to be spectrally dependent, as discussed in previous sections. Therefore, we also determined $k^{II}_{OH,eff}$ and $\tau_{1/2,\ cloud\text{-}water}$ based on changes in absorbance at 400 nm (Fig. S11 and Table S6†). We found that $k^{II}_{OH,eff}$ and $\tau_{1/2,\ cloud\text{-}water}$ values for all three solid biomass fuel burning types corresponding to 365 nm and 400 nm wavelengths were found statistically comparable using a two-tail *t*-test ($p > 0.05$). These results indicate that solid biomass fuel burning BrC aerosols in the atmospheric aqueous phases may undergo OH oxidation at similar rates, regardless of their source fuel and wavelength of absorbance measurements used to calculate $k^{II}_{OH,eff}$.

4. Conclusions and environmental implications

Atmospheric BrC aerosols are short-lived climate pollutants contributing to both air pollution and global warming. The atmospheric warming effect of BrC aerosols has become emergent in recent years, constituting ~7 to 48% of total anthropogenic aerosol warming globally.[1,2] This contribution could be as high as ~40 to 50% in highly polluted and biomass burning dominated environments such as South Asia.[12,14,72–74] However, due to limited investigations on biomass fuel burning types that are relevant to these areas, the exact climatic impacts of aqueous-phase processing of BrC over these regions is poorly understood. Our study is the first to assess the photochemical aging of emissions arising from cow dung burning, a type of solid biomass fuel widely used in middle- and low-income countries. The BrC species arising from solid biomass fuel burning investigated here are susceptible to changes in their absorbance and composition through numerous atmospherically relevant photochemical processes (*i.e.*, direct photolysis and OH oxidation). The experimental conditions used in this study best describe changes occurring inside clouds and foggy droplets due to photochemical oxidation, which result in

changes in the absorbance and composition of biomass burning BrC aerosols.

The aqueous-phase direct photolysis of WS-BrC aerosols caused significant changes in their absorbance, absorptivity and chemical composition. Three different types of UV-lights were employed for direct photolysis, *i.e.*, UVB(Q), UVB(G) and UVA(Q), placed in the order of emission spectra from shorter to longer wavelengths. We observed that the extent of photo-enhancement in WS-BrC absorbance is most likely to increase upon exposure to shorter-wavelength UV-light, whereas more intense photobleaching is likely during longer wavelength UV-light based direct photolysis in aqueous media such as clouds and fog droplets. The photo-enhancement in WS-BrC absorbance coincided with oligomer formation. Previous studies[75,76] have reported that countries located between −30°N and 30°N, home for ∼80% global population, have the most exposure to UV radiation. A major fraction of this UV radiation (>90%) fell in the 320 to 400 nm solar spectrum.[34,35] These points signify the atmospheric relevance of the aqueous-phase direct photolysis process, especially corresponding to UVB(G) and UVA(Q), explored in this study. Moreover, the dependence of BrC evolution on the wavelength of irradiation in direct photolysis can have implications on their fate in the atmosphere, especially in clouds and fog droplets, and therefore, needs to be further studied.

The aqueous-phase OH oxidation experiments showed similar second-order rate constant values for dung cake and wood burning, suggesting that the fate of WS-BrC in clouds and fog droplets may not depend on the biomass type. This finding is crucial as different biomass burning types dominate the BrC budget in different parts of the world, for example, agriculture residue,[12,73] dung cake[13] and wood[13] burning in South Asia; wood burning/wildfires in North and South America,[67,77] bushfires in Australia,[78] *etc.* Additionally, insignificant differences were found in the second-order rate constant values calculated corresponding to the changes in absorbance at two different wavelengths, implying the rationality of single-wavelength based photochemical bleaching models in the aqueous medium. This study focused on photochemical aging of WSOC aerosols, representing an ∼80% fraction of total OC,[29] produced from the pyrolysis of solid biomass fuels. However, biomass burning conditions in the actual atmosphere might be different from pyrolysis. The physico-chemical and optical properties of freshly emitted BrC particles have been reported to depend on their burn conditions.[17,79] Moreover, in addition to in-cloud exposure, an air mass can also be exposed to heterogeneous photochemical oxidation. Therefore, we propose that future studies should be centered on understanding the evolution and fate of BrC emitted from burning of different biomass types (*e.g.*, dung cakes, agriculture residues, wood, *etc.*) under different burning conditions in atmospherically relevant oxidation processes.

Furthermore, aqueous-phase OH oxidation experiments for dung cake and wood burning also revealed that the bleaching of WS-BrC (light-absorbing fraction of WSOC) in clouds/fog is ∼1 order of magnitude faster than scavenging of total WSOC ($k^{II}_{OH,eff} = 1.8 \times 10^8$).[71] These findings emphasize that BrC and OC should be treated as separate entities (although BrC is a fraction of OC) in global climate models, though the dynamic equilibrium should be maintained between the two, to mitigate/constrain uncertainties in radiative forcing estimates for BrC, especially indirect radiative forcing.

Conflicts of interest

There are no conflicts of interest to declare.

Acknowledgements

The authors thank Dr Gregory Kiema for his assistance with UV-vis spectroscopy, the University of Alberta MS facility and the Natural Resources Analytical Laboratory for their assistance with LC-MS and TOC-TN analyses, as well as the Rangeland Research Institute at the University of Alberta for providing CAD dung samples. We also acknowledge financial support from the Science and Engineering Research Board (SERB) in the Department of Science and Technology of the Government of India (Grant# SB/S9/Z-16/2016-VI (2019–2020)), the Canada Foundation of Innovation (Project Number 38334) and the NSERC Discovery Grant (RGPIN2018-03814), IIT Kanpur and the University of Alberta.

References

1 L. Zeng, A. Zhang, Y. Wang, N. L. Wagner, J. M. Katich, J. P. Schwarz, G. P. Schill, C. Brock, K. D. Froyd, D. M. Murphy, C. J. Williamson, A. Kupc, E. Scheuer, J. Dibb and R. J. Weber, Global Measurements of Brown Carbon and Estimated Direct Radiative Effects, *Geophys. Res. Lett.*, 2020, **47**, e2020GL088747.

2 Y. Feng, V. Ramanathan and V. R. Kotamarthi, Brown carbon: A significant atmospheric absorber of solar radiation, *Atmos. Chem. Phys.*, 2013, **13**, 8607–8621.

3 A. Hecobian, X. Zhang, M. Zheng, N. Frank, E. S. Edgerton and R. J. Weber, Water-soluble organic aerosol material and the light-absorption characteristics of aqueous extracts measured over the Southeastern United States, *Atmos. Chem. Phys.*, 2010, **10**, 5965–5977.

4 M. O. Andreae and A. Gelencsér, Black carbon or brown carbon? the nature of light-absorbing carbonaceous aerosols, *Atmos. Chem. Phys.*, 2006, **6**, 3131–3148.

5 M. Z. Jacobson, Isolating nitrated and aromatic aerosols and nitrated aromatic gases as sources of ultraviolet light absorption, *J. Geophys. Res.: Atmos.*, 1999, **104**, 3527–3542.

6 J. Mok, N. A. Krotkov, A. Arola, O. Torres, H. Jethva, M. Andrade, G. Labow, T. F. Eck, Z. Li, R. R. Dickerson, G. L. Stenchikov, S. Osipov and X. Ren, Impacts of brown carbon from biomass burning on surface UV and ozone photochemistry in the Amazon Basin, *Sci. Rep.*, 2016, **6**, 1–9.

7 R. F. Hems, E. G. Schnitzler, C. Liu-Kang, C. D. Cappa and J. P. D. Abbatt, Aging of Atmospheric Brown Carbon Aerosol, *ACS Earth Space Chem.*, 2021, **5**, 722–748.

8 Ö. Gustafsson and V. Ramanathan, Convergence on climate warming by black carbon aerosols, *Proc. Natl. Acad. Sci. U. S. A.*, 2016, **113**, 4243–4245.
9 A. Laskin, J. Laskin and S. A. Nizkorodov, Chemistry of Atmospheric Brown Carbon, *Chem. Rev.*, 2015, **115**, 4335–4382.
10 X. Wang, C. L. Heald, D. A. Ridley, J. P. Schwarz, J. R. Spackman, A. E. Perring, H. Coe, D. Liu and A. D. Clarke, Exploiting simultaneous observational constraints on mass and absorption to estimate the global direct radiative forcing of black carbon and brown carbon, *Atmos. Chem. Phys.*, 2014, **14**, 10989–11010.
11 R. A. Di Lorenzo, B. K. Place, T. C. VandenBoer and C. J. Young, Composition of Size-Resolved Aged Boreal Fire Aerosols: Brown Carbon, Biomass Burning Tracers, and Reduced Nitrogen, *ACS Earth Space Chem.*, 2018, **2**, 278–285.
12 V. Choudhary, G. K. Singh, T. Gupta and D. Paul, Absorption and radiative characteristics of brown carbon aerosols during crop residue burning in the source region of Indo-Gangetic Plain, *Atmos. Res.*, 2021, **249**, 105285.
13 A. Pandey, S. Pervez and R. K. Chakrabarty, Filter-based measurements of UV-vis mass absorption cross sections of organic carbon aerosol from residential biomass combustion: Preliminary findings and sources of uncertainty, *J. Quant. Spectrosc. Radiat. Transfer*, 2016, **182**, 296–304.
14 E. N. Kirillova, A. Andersson, S. Tiwari, A. K. Srivastava, D. S. Bisht and Ö. Gustafsson, Water-soluble organic carbon aerosols during a full New Delhi winter: Isotope-based source apportionment and optical properties, *J. Geophys. Res.*, 2014, **119**, 3476–3485.
15 C. Yan, M. Zheng, C. Bosch, A. Andersson, Y. Desyaterik, A. P. Sullivan, J. L. Collett, B. Zhao, S. Wang, K. He and Ö. Gustafsson, Important fossil source contribution to brown carbon in Beijing during winter, *Sci. Rep.*, 2017, **7**, 1–10.
16 J. P. S. Wong, M. Tsagkaraki, I. Tsiodra, N. Mihalopoulos, K. Violaki, M. Kanakidou, J. Sciare, A. Nenes and R. J. Weber, Atmospheric evolution of molecular-weight-separated brown carbon from biomass burning, *Atmos. Chem. Phys.*, 2019, **19**, 7319–7334.
17 R. Saleh, E. S. Robinson, D. S. Tkacik, A. T. Ahern, S. Liu, A. C. Aiken, R. C. Sullivan, A. A. Presto, M. K. Dubey, R. J. Yokelson, N. M. Donahue and A. L. Robinson, Brownness of organics in aerosols from biomass burning linked to their black carbon content, *Nat. Geosci.*, 2014, **7**, 647–650.
18 R. Saleh, C. J. Hennigan, G. R. McMeeking, W. K. Chuang, E. S. Robinson, H. Coe, N. M. Donahue and A. L. Robinson, Absorptivity of brown carbon in fresh and photo-chemically aged biomass-burning emissions, *Atmos. Chem. Phys.*, 2013, **13**, 7683–7693.
19 Y. Chen and T. C. Bond, Light absorption by organic carbon from wood combustion, *Atmos. Chem. Phys.*, 2010, **10**, 1773–1787.
20 World Health Organization (WHO), *Golbal Househ. Energy Database*.
21 C. Venkataraman, A. D. Sagar, G. Habib, N. Lam and K. R. Smith, The Indian National Initiative for Advanced Biomass Cookstoves: The benefits of clean combustion, *Energy Sustainable Dev.*, 2010, **14**, 63–72.
22 L. T. Fleming, P. Lin, A. Laskin, J. Laskin, R. Weltman, R. D. Edwards, N. K. Arora, A. Yadav, S. Meinardi, D. R. Blake, A. Pillarisetti, K. R. Smith and S. A. Nizkorodov, Molecular composition of particulate matter emissions from dung and brushwood burning household cookstoves in Haryana, India, *Atmos. Chem. Phys.*, 2018, **18**, 2461–2480.
23 S. Philip, R. V. Martin, A. Van Donkelaar, J. W. H. Lo, Y. Wang, D. Chen, L. Zhang, P. S. Kasibhatla, S. Wang, Q. Zhang, Z. Lu, D. G. Streets, S. Bittman and D. J. Macdonald, Global chemical composition of ambient fine particulate matter for exposure assessment, *Environ. Sci. Technol.*, 2014, **48**, 13060–13068.
24 A. Pandey, P. Sadavarte, A. B. Rao and C. Venkataraman, Trends in multi-pollutant emissions from a technology-linked inventory for India: II. Residential, agricultural and informal industry sectors, *Atmos. Environ.*, 2014, **99**, 341–352.
25 F. Karagulian, C. A. Belis, C. F. C. Dora, A. M. Prüss-Ustün, S. Bonjour, H. Adair-Rohani and M. Amann, Contributions to cities' ambient particulate matter (PM): A systematic review of local source contributions at global level, *Atmos. Environ.*, 2015, **120**, 475–483.
26 A. Chakraborty, P. Rajeev, P. Rajput and T. Gupta, Water soluble organic aerosols in indo gangetic plain (IGP): Insights from aerosol mass spectrometry, *Sci. Total Environ.*, 2017, **599–600**, 1573–1582.
27 S. Sharma, M. Chandra and S. Harsha Kota, Four year long simulation of carbonaceous aerosols in India: Seasonality, sources and associated health effects, *Environ. Res.*, 2022, **213**, 113676.
28 R. F. Hems, E. G. Schnitzler, M. Bastawrous, R. Soong, A. J. Simpson and J. P. D. Abbatt, Aqueous Photoreactions of Wood Smoke Brown Carbon, *ACS Earth Space Chem.*, 2020, **4**, 1149–1160.
29 J. P. S. Wong, A. Nenes and R. J. Weber, Changes in Light Absorptivity of Molecular Weight Separated Brown Carbon Due to Photolytic Aging, *Environ. Sci. Technol.*, 2017, **51**, 8414–8421.
30 R. Zhao, A. K. Y. Lee, L. Huang, X. Li, F. Yang and J. P. D. Abbatt, Photochemical processing of aqueous atmospheric brown carbon, *Atmos. Chem. Phys.*, 2015, **15**, 6087–6100.
31 V. Choudhary, T. Gupta and R. Zhao, Evolution of Brown Carbon Aerosols during Atmospheric Long-Range Transport in the South Asian Outflow and Himalayan Cryosphere, *ACS Earth Space Chem.*, 2022, **6**, 2335–2347.
32 V. Choudhary, P. Rajput and T. Gupta, Absorption properties and forcing efficiency of light-absorbing water-soluble organic aerosols: Seasonal and spatial variability, *Environ. Pollut.*, 2021, **272**, 115932.
33 H. Forrister, J. Liu, E. Scheuer, J. Dibb, L. Ziemba, K. L. Thornhill, B. Anderson, G. Diskin, A. E. Perring,

J. P. Schwarz, P. Campuzano-Jost, D. A. Day, B. B. Palm, J. L. Jimenez, A. Nenes and R. J. Weber, Evolution of brown carbon in wildfire plumes, *Geophys. Res. Lett.*, 2015, **42**, 4623–4630.

34 Y. Zhou, X. Meng, J. H. Belle, H. Zhang, C. Kennedy, M. Z. Al-Hamdan, J. Wang and Y. Liu, Compilation and spatio-temporal analysis of publicly available total solar and UV irradiance data in the contiguous United States, *Environ. Pollut.*, 2019, **253**, 130–140.

35 D. L. Narayanan, R. N. Saladi and J. L. Fox, Ultraviolet radiation and skin cancer, *Int. J. Dermatol.*, 2010, **49**, 978–986.

36 B. R. T. Simoneit, Biomass burning – A review of organic tracers for smoke from incomplete combustion, *Appl. Geochem.*, 2002, **17**, 129–162.

37 M. Loebel Roson, R. Duruisseau-Kuntz, M. Wang, K. Klimchuk, R. J. Abel, J. J. Harynuk and R. Zhao, Chemical Characterization of Emissions Arising from Solid Fuel Combustion – Contrasting Wood and Cow Dung Burning, *ACS Earth Space Chem.*, 2021, **5**, 2925–2937.

38 P. Lin, L. T. Fleming, S. A. Nizkorodov, J. Laskin and A. Laskin, Comprehensive Molecular Characterization of Atmospheric Brown Carbon by High Resolution Mass Spectrometry with Electrospray and Atmospheric Pressure Photoionization, *Anal. Chem.*, 2018, **90**, 12493–12502.

39 P. Lin, N. Bluvshtein, Y. Rudich, S. A. Nizkorodov, J. Laskin and A. Laskin, Molecular Chemistry of Atmospheric Brown Carbon Inferred from a Nationwide Biomass Burning Event, *Environ. Sci. Technol.*, 2017, **51**, 11561–11570.

40 R. P. Pokhrel, J. Gordon, M. N. Fiddler and S. Bililign, Impact of combustion conditions on physical and morphological properties of biomass burning aerosol, *Aerosol Sci. Technol.*, 2021, **55**, 80–91.

41 R. P. Pokhrel, J. Gordon, M. N. Fiddler and S. Bililign, Determination of Emission Factors of Pollutants From Biomass Burning of African Fuels in Laboratory Measurements, *J. Geophys. Res.: Atmos.*, 2021, **126**, 1–17.

42 Y. H. Kim, C. King, T. Krantz, M. M. Hargrove, I. J. George, J. McGee, L. Copeland, M. D. Hays, M. S. Landis, M. Higuchi, S. H. Gavett and M. I. Gilmour, The role of fuel type and combustion phase on the toxicity of biomass smoke following inhalation exposure in mice, *Arch. Toxicol.*, 2019, **93**, 1501–1513.

43 E. S. Galbavy, K. Ram and C. Anastasio, 2-Nitrobenzaldehyde as a chemical actinometer for solution and ice photochemistry, *J. Photochem. Photobiol., A*, 2010, **209**, 186–192.

44 T. Schaefer, L. Wen, A. Estelmann, J. Maak and H. Herrmann, pH-and temperature-dependent kinetics of the oxidation reactions of OH with succinic and pimelic acid in aqueous solution, *Atmosphere*, 2020, **11**, 17–24.

45 H. Herrmann, D. Hoffmann, T. Schaefer, P. Bräuer and A. Tilgner, Tropospheric aqueous-phase free-radical chemistry: Radical sources, spectra, reaction kinetics and prediction tools, *ChemPhysChem*, 2010, **11**, 3796–3822.

46 B. Ervens, S. Gligorovski and H. Herrmann, Temperature-dependent rate constants for hydroxyl radical reactions with organic compounds in aqueous solutions, *Phys. Chem. Chem. Phys.*, 2003, **5**, 1811–1824.

47 N. Sedehi, H. Takano, V. A. Blasic, K. A. Sullivan and D. O. De Haan, Temperature- and pH-dependent aqueous-phase kinetics of the reactions of glyoxal and methylglyoxal with atmospheric amines and ammonium sulfate, *Atmos. Environ.*, 2013, **77**, 656–663.

48 H. Che, M. Segal-Rozenhaimer, L. Zhang, C. Dang, P. Zuidema, A. Dobracki, A. J. Sedlacek, H. Coe, H. Wu, J. Taylor, X. Zhang, J. Redemann and J. Haywood, Cloud processing and weeklong ageing affect biomass burning aerosol properties over the south-eastern Atlantic, *Commun. Earth Environ.*, 2022, **3**, 1–9.

49 J. V. Amorim, S. Wu, K. Klimchuk, C. Lau, F. J. Williams, Y. Huang and R. Zhao, PH Dependence of the OH Reactivity of Organic Acids in the Aqueous Phase, *Environ. Sci. Technol.*, 2020, **54**, 12484–12492.

50 R. Zhao, A. K. Y. Lee, R. Soong, A. J. Simpson and J. P. D. Abbatt, Formation of aqueous-phase α-hydroxyhydroperoxides (α-HHP): Potential atmospheric impacts, *Atmos. Chem. Phys.*, 2013, **13**, 5857–5872.

51 J. M. St. Clair, J. C. Rivera-Rios, J. D. Crounse, H. C. Knap, K. H. Bates, A. P. Teng, S. Jorgensen, H. G. Kjaergaard, F. N. Keutsch and P. O. Wennberg, Kinetics and Products of the Reaction of the First-Generation Isoprene Hydroxy Hydroperoxide (ISOPOOH) with OH, *J. Phys. Chem. A*, 2016, **120**, 1441–1451.

52 C. N. Satterfield and L. C. Case, Reaction of Aldehyde and Hydrogen Peroxide in Aqueous Solution, *Ind. Eng. Chem.*, 1954, **46**, 998–1001.

53 S. Wu, E. Kim, D. Vethanayagam and R. Zhao, Indoor partitioning and potential thirdhand exposure to carbonyl flavoring agents added in e-cigarette and hookah tobacco, *Environ. Sci.: Processes Impacts*, 2022, 2294–2309.

54 E. Yeshno, O. Dahan, S. Bernstain and S. Arnon, A novel analytical approach for the simultaneous measurement of nitrate and dissolved organic carbon in soil water, *Hydrol. Earth Syst. Sci.*, 2021, **25**, 2159–2168.

55 D. Sengupta, V. Samburova, C. Bhattarai, E. Kirillova, L. Mazzoleni, M. Iaukea-Lum, A. Watts, H. Moosmüller and A. Khlystov, Light absorption by polar and non-polar aerosol compounds from laboratory biomass combustion, *Atmos. Chem. Phys.*, 2018, **18**, 10849–10867.

56 P. Lin, N. Bluvshtein and A. Laskin, Molecular Chemistry of Atmospheric Brown Carbon Inferred from a Nationwide Biomass Burning Event, *Environ. Sci. Technol.*, 2017, 11561–11570.

57 M. Lyu, D. K. Thompson, N. Zhang, C. W. Cuss, C. J. Young and S. A. Styler, Unraveling the complexity of atmospheric brown carbon produced by smoldering boreal peat using size-exclusion chromatography with selective mobile phases, *Environ. Sci.: Atmos.*, 2021, **1**, 241–252.

58 R. A. Di Lorenzo and C. J. Young, Size separation method for absorption characterization in brown carbon: Application to an aged biomass burning sample, *Geophys. Res. Lett.*, 2016, **43**, 458–465.

59 K. D. Duncan, G. W. Vandergrift, E. T. Krogh and C. G. Gill, Ionization suppression effects with condensed phase membrane introduction mass spectrometry: Methods to increase the linear dynamic range and sensitivity, *J. Mass Spectrom.*, 2014, **50**, 437–443.

60 K. D. Duncan, J. A. Hawkes, M. Berg, B. Clarijs, C. G. Gill, J. Bergquist, I. Lanekoff and E. T. Krogh, Membrane Sampling Separates Naphthenic Acids from Biogenic Dissolved Organic Matter for Direct Analysis by Mass Spectrometry, *Environ. Sci. Technol.*, 2022, **56**, 3096–3105.

61 J. Monaghan, L. C. Richards, G. W. Vandergrift, L. J. Hounjet, S. R. Stoyanov, C. G. Gill and E. T. Krogh, Direct mass spectrometric analysis of naphthenic acids and polycyclic aromatic hydrocarbons in waters impacted by diluted bitumen and conventional crude oil, *Sci. Total Environ.*, 2021, **765**, 144206.

62 G. W. Vandergrift, W. Lattanzio-Battle, T. R. Rodgers, J. B. Atkinson, E. T. Krogh and C. G. Gill, Geospatial Assessment of Trace-Level Benzophenone-3 in a Fish-Bearing River Using Direct Mass Spectrometry, *ACS Environ. Sci. Technol. Water*, 2022, **2**, 262–267.

63 L. Yu, J. Smith, A. Laskin, C. Anastasio, J. Laskin and Q. Zhang, Chemical characterization of SOA formed from aqueous-phase reactions of phenols with the triplet excited state of carbonyl and hydroxyl radical, *Atmos. Chem. Phys.*, 2014, **14**, 13801–13816.

64 Q. Zhang, Y. Zhang, Z. Wu, B. Zhang, Y. Zeng, J. Sun, H. Xu, Z. Li, J. Cao and Z. Shen, Enhanced behaviors of optical properties and the radiative effects of molecular-specific brown carbon from dung combustion in the Tibetan Plateau, *Atmos. Chem. Phys.*, DOI: **10.5194/acp-2022-801**.

65 R. Satish, N. Rastogi, A. Singh and D. Singh, Change in characteristics of water-soluble and water-insoluble brown carbon aerosols during a large-scale biomass burning, *Environ. Sci. Pollut. Res.*, 2020, **27**, 33339–33350.

66 J. D. Smith, H. Kinney and C. Anastasio, Phenolic carbonyls undergo rapid aqueous photodegradation to form low-volatility, light-absorbing products, *Atmos. Environ.*, 2016, **126**, 36–44.

67 R. A. Di Lorenzo, R. A. Washenfelder, A. R. Attwood, H. Guo, L. Xu, N. L. Ng, R. J. Weber, K. Baumann, E. Edgerton and C. J. Young, Molecular-Size-Separated Brown Carbon Absorption for Biomass-Burning Aerosol at Multiple Field Sites, *Environ. Sci. Technol.*, 2017, **51**, 3128–3137.

68 J. J. Schauer, M. J. Kleeman, G. R. Cass and B. R. T. Simoneit, Measurement of emissions from air pollution sources. 3. C1-C29 organic compounds from fireplace combustion of wood, *Environ. Sci. Technol.*, 2001, **35**, 1716–1728.

69 R. F. Hems and J. P. D. Abbatt, Aqueous Phase Photo-oxidation of Brown Carbon Nitrophenols: Reaction Kinetics, Mechanism, and Evolution of Light Absorption, *ACS Earth Space Chem.*, 2018, **2**, 225–234.

70 C. Mohr, F. D. Lopez-Hilfiker, P. Zotter, A. S. H. Prévoît, L. Xu, N. L. Ng, S. C. Herndon, L. R. Williams, J. P. Franklin, M. S. Zahniser, D. R. Worsnop, W. B. Knighton, A. C. Aiken, K. J. Gorkowski, M. K. Dubey, J. D. Allan and J. A. Thornton, Contribution of nitrated phenols to wood burning brown carbon light absorption in detling, united kingdom during winter time, *Environ. Sci. Technol.*, 2013, **47**, 6316–6324.

71 T. Arakaki, C. Anastasio, Y. Kuroki, H. Nakajima, K. Okada, Y. Kotani, D. Handa, S. Azechi, T. Kimura, A. Tsuhako and Y. Miyagi, A general scavenging rate constant for reaction of hydroxyl radical with organic carbon in atmospheric waters, *Environ. Sci. Technol.*, 2013, **47**, 8196–8203.

72 V. Choudhary, P. Rajput, D. K. Singh, A. K. Singh and T. Gupta, Light absorption characteristics of brown carbon during foggy and non-foggy episodes over the Indo-Gangetic Plain, *Atmos. Pollut. Res.*, 2018, **9**, 494–501.

73 B. Srinivas, N. Rastogi, M. M. Sarin, A. Singh and D. Singh, Mass absorption efficiency of light absorbing organic aerosols from source region of paddy-residue burning emissions in the Indo-Gangetic Plain, *Atmos. Environ.*, 2016, **125**, 360–370.

74 C. E. Chung, V. Ramanathan and D. Decremer, Observationally constrained estimates of carbonaceous aerosol radiative forcing, *Proc. Natl. Acad. Sci. U. S. A.*, 2012, **109**, 11624–11629.

75 J. Grobner, *Encyclopedia of Sustainability Science and Technology*, Springer, New York, NY, 2012.

76 A. Tanskanen, N. A. Krotkov, J. R. Herman and A. Arola, Surface ultraviolet irradiance from OMI, *IEEE Trans. Geosci. Remote Sens.*, 2006, **44**, 1267–1271.

77 A. Hoffer, A. Gelencsér, P. Guyon, G. Kiss, O. Schmid, G. P. Frank, P. Artaxo and M. O. Andreae, Optical properties of humic-like substances (HULIS) in biomass-burning aerosols, *Atmos. Chem. Phys.*, 2006, **6**, 3563–3570.

78 B. Norman, P. Newman and W. Steffen, Apocalypse now: Australian bushfires and the future of urban settlements, *npj Urban Sustain.*, 2021, **1**, 1–9.

79 Z. Lu, D. G. Streets, E. Winijkul, F. Yan, Y. Chen, T. C. Bond, Y. Feng, M. K. Dubey, S. Liu, J. P. Pinto and G. R. Carmichael, Light absorption properties and radiative effects of primary organic aerosol emissions, *Environ. Sci. Technol.*, 2015, **49**, 4868–4877.